Moritz Boueke, Johannes Hoffmann, Tobias Schmidt, Christin Bald, Robert Bergholz, and Gerhard Schmidt*

Model-based Tracking of Magnetic Sensor Gloves in Real Time

https://doi.org/10.1515/cdbme-2023-1022

Abstract: While mechanical tracking is commonly seen in robot-assisted surgery, contactless gesture control leads to a more intuitive approach. Magnetic localization systems might be able to provide an untethered access to the necessary hand movement data. A model-based system exploiting a priori knowledge to improve the accuracy and robustness can be beneficial in this context. We present a proof of concept, in which the index finger of a digital twin of a hand is tracked with three simulated sensors. Based on the physiological composition, the finger is modeled as a kinematic chain with rotational degrees of freedom between the segments according to the corresponding finger joints. We applied an extended Kalman filter using this description to enhance position and rotation estimates for the sensors on the finger segments. We achieved mean absolute errors $< 1\,\mathrm{cm}$ for the positions and $< 10^\circ$ for the local rotations with first simulations of a bending motion.

Keywords: Extended Kalman filter, kinematic chain, pose estimation, robot-assisted surgery

1 Introduction

Motion tracking of the hands is of high interest for control purposes in robot-assisted surgery. While currently performed by mechanical means, such as terminal-mounted controllers, a contact-free approach using sensor gloves could make this more intuitive as the hands can be moved more freely in a contained operating space and a broader range of gestures might be used in the control of the robot system. This could be achieved for example using flexure sensors [1], optical systems [2] or, as explored here, magnetic sensors.

Localization of 3D magnetic sensors has already been well established with different approaches (cf. [3–5]) and is a possible application for novel magnetoelectric sensors which are cost-efficient and highly sensitive [6]. This contribution is meant to enable and enhance such approaches by a model-based system as shown in Figure 1 that incorporates a priori knowledge about the hand and utilizes it for the tracking of a magnetic sensor glove.

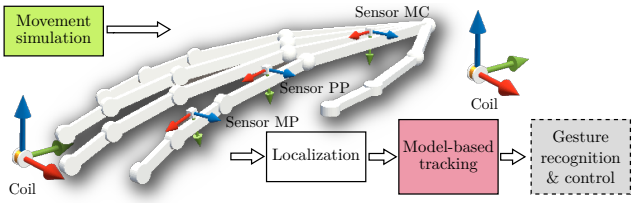

Figure 1: Overview of the hand sensor tracking system.

2 Methods

As depicted in Figure 2, the investigated model-based estimator forms the end of a comprehensive processing pipeline which we explore in the following.

Hand Simulation

To validate our tracking approach, the hand simulation is currently comprised of a cycle of a bending and corresponding unbending motion, as it might be used for pointing or - when used with multiple fingers - a gripping movement, which is of interest for the use in robot-assisted surgery. This is achieved by actuating the local segments with a sinusoidal s-curve, starting from a resting position of 0° to 70° for the metacarpal (MC) while the proximal phalanx (PP) of the index finger is moved from 10° to 60° and the medial phalanx (MP) is rotated from 10° to 105°. An inverse of this motion is afterwards applied which forms the course of one cycle.

This digital twin is equipped with three simulated sensors, situated on the MC, PP and MP of the index finger, respectively. We assumed the lengths of the finger segments of interest based on values from [7] which are $l_{01} = 6.8\,\mathrm{cm}$ for the MC and $l_{12} = 4.0\,\mathrm{cm}$ for the PP. Sensor placement on these segments is described by vectors in local coordinate frames. The local coordinate systems are placed at the finger joints and rotated such that the x-axis points along the following bone towards the tip of the finger, the z-axis is the axis around which the flexion/extension of the joint happens and the y-axis

***Corresponding author: Gerhard Schmidt,** Digital Signal Processing and System Theory, Department of Electrical and Information Engineering, Faculty of Engineering, Kiel University, Kaiserstr. 2, 24143 Kiel, Germany, gus@tf.uni-kiel.de
Moritz Boueke, Johannes Hoffmann, Tobias Schmidt, Christin Bald, Department of Electrical and Information Engineering, Faculty of Engineering, Kiel University, Kiel, Germany
Robert Bergholz, Department of Pediatric Surgery, Faculty of Medicine, Kiel University, Kiel, Germany

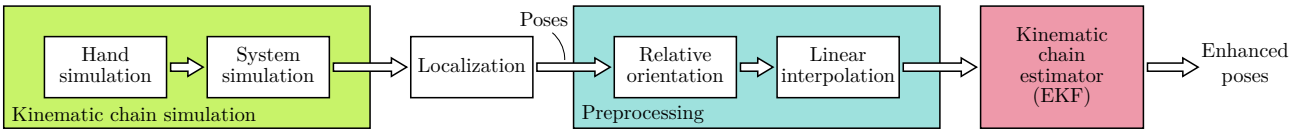

Figure 2: Overview over the relevant parts of the model-based system.

is such that the resulting coordinate frame is a right-hand system. Accordingly, this means that the abduction/adduction of a joint capable of that motion revolves around this axis. In Figure 1, the resulting local frames for the sensors can also be seen.

Kinematic Chain

A key concept in the further processing revolves around the idea of treating the index finger as a kinematic chain. With the knowledge of the (local) orientation at each joint and the lengths of the digits as well as vectors to the sensors (which can be considered as the end-effectors for this case), we can reconstruct the position of each sensor. This concept is depicted in Figure 3 for a two dimensional chain, which can be seen as the index finger when only moved in one plane. From this, the relation between the position of the PPs' sensor $\boldsymbol{p}_1$ (here directly in line with the segment) can easily be found as

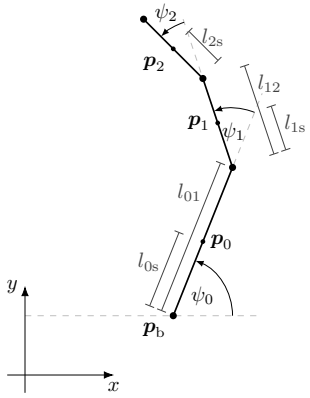

Figure 3: Conceptual representation of a kinematic chain in 2D.

$$\boldsymbol{p}_1 = \begin{bmatrix} l_{1s}\cos(\psi_0+\psi_1) + l_{01}\cos(\varphi_0) + x_\mathrm{b} \\ l_{1s}\sin(\psi_0+\psi_1) + l_{01}\sin(\psi_0) + y_\mathrm{b} \end{bmatrix}, \qquad (1)$$

with simple trigonometric relationships and the base of the chain $\boldsymbol{p}_\mathrm{b} = [x_\mathrm{b}\ \ y_\mathrm{b}]^\mathrm{T}$ assumed known. This equation obviously gets more lengthy with each chain element, but the general concept is independent from the number of segments.

Since descriptions of rotations in 3D space are much more complex, the described relation (see (1)) gets more difficult. We decided to represent the rotation in roll (φ), pitch (θ), and yaw (ψ) angles around the x-, y-, and z-axis respectively, as this formulation is the most intuitive to grasp. However, as these angles are prone to the problem of gimbal lock, we used unit quaternions in the four dimensional set $\mathbb{H}$ for rotation representation in the actual calculations regarding the kinematic chain. Here, $\otimes$ denotes the quaternion multiplication, $\boldsymbol{q} \in \mathbb{H}$ are quaternions where the subscript indicates which two coordinate frames the rotation relates to each other and $(\cdot)^*$ is the conjugate operation. In the subscripts, g represents the global reference frame and b the base frame located at the wrist and rotated by a fixed and known base orientation ($\varphi_\mathrm{b} = -90°$, $\theta_\mathrm{b} = \psi_\mathrm{b} = 0°$) for consistency between the local segments' coordinate frames. For the same example of the PPs' sensor, we use the unit quaternions $\boldsymbol{q}_\mathrm{g1}$ and $\boldsymbol{q}_\mathrm{g0}$ calculated from the global orientations of sensor PP and MC respectively in the resulting relation

$$\begin{bmatrix} 0 \\ \boldsymbol{p}_1 \end{bmatrix} = \boldsymbol{q}_\mathrm{g1} \otimes \begin{bmatrix} 0 \\ \boldsymbol{l}_\mathrm{1s} \end{bmatrix} \otimes \boldsymbol{q}_\mathrm{g1}^* + \boldsymbol{q}_\mathrm{g0} \otimes \begin{bmatrix} 0 \\ l_{01} \\ 0 \\ 0 \end{bmatrix} \otimes \boldsymbol{q}_\mathrm{g0}^* + \begin{bmatrix} 0 \\ \boldsymbol{p}_\mathrm{b} \end{bmatrix} \qquad (2)$$

with

$$\boldsymbol{q}_\mathrm{g1} = \boldsymbol{q}_\mathrm{gb} \otimes \boldsymbol{q}_\mathrm{b0} \otimes \boldsymbol{q}_{01}, \quad \boldsymbol{q}_\mathrm{g0} = \boldsymbol{q}_\mathrm{gb} \otimes \boldsymbol{q}_\mathrm{b0}. \qquad (3)$$

Localization

To simulate a possible localization algorithm based on actuator coils exciting a known magnetic field that is prone to errors and has a longer time between pose results, the ground truth signals are subsampled. The time between samples is chosen as $96\,\mathrm{ms}$ in accordance to the frequency of new localization results in the actual signal processing chain presented in [3, 4]. Furthermore, the same experimental constraints (tracking space of $50\,\mathrm{cm} \times 50\,\mathrm{cm} \times 20\,\mathrm{cm}$) are assumed. To model localization errors, these signals were then superimposed with additive white Gaussian noise with standard deviations of $2\,\mathrm{cm}$ for the positions and $10°$ for the orientation respectively.

Preprocessing

During preprocessing, the measured orientations in global coordinates are first mapped to their corresponding orientations in the segment based coordinate frames. This is achieved by calculating the orientation quaternions for each incoming set of roll-pitch-yaw angles, multiplying it from the left with the preceding, conjugated orientation quaternion and reforming the roll-pitch-yaw representation from the result. Furthermore, to enable the use of a quasi-continuous discrete system model, we linearly interpolate the incoming signals to achieve a typical working samplerate of $1\,\mathrm{kHz}$ for the subsequent Kalman filter.

Extended Kalman Filter

Forming the core of the present work is an extended Kalman filter (EKF), which models the inertia in the tracked movement and, more importantly, fuses the redundant information of the localized positions and orientations in a beneficial way while incorporating the a priori knowledge about the kinematic chain-like nature of the index finger and the physiological limitations of its joints. The latter is done by restricting the degrees of freedom of each joint. Since the metacarpophalangeal joint can only perform flexion/extension and abduction/adduction movements, only the local pitch and yaw are taken into account. Using the same reasoning, we only model the yaw angle in the rotation from the proximal to the medial placed sensor. Hence, we formulate the state vector $\boldsymbol{x} \in \mathbb{R}^{15}$ as

$$\boldsymbol{x}(n) = \begin{bmatrix} \boldsymbol{\alpha}^{\mathrm{T}}(n) & \dot{\boldsymbol{\alpha}}^{\mathrm{T}}(n) & \boldsymbol{p}_{\mathrm{b}}^{\mathrm{T}}(n) \end{bmatrix}^{\mathrm{T}}, \tag{4}$$

$$\boldsymbol{\alpha}(n) = \begin{bmatrix} \varphi_0(n) & \theta_0(n) & \psi_0(n) & \theta_1(n) & \psi_1(n) & \psi_2(n) \end{bmatrix}^{\mathrm{T}} \tag{5}$$

with the vector $\boldsymbol{\alpha}$ containing the angles under consideration and the time index n. We describe the system's state propagation linearly using the system matrix $\boldsymbol{A}$ and an input matrix $\boldsymbol{B}$ coupling in the base's position

$$\boldsymbol{A} = \begin{bmatrix} \boldsymbol{I}_6 & \boldsymbol{I}_6 \cdot T_{\mathrm{s}} & \boldsymbol{0}_{3\times3} \\ \boldsymbol{0}_{6\times6} & \boldsymbol{I}_6 & \boldsymbol{0}_{3\times3} \\ & \boldsymbol{0}_{3\times15} & \end{bmatrix}, \quad \boldsymbol{B} = \begin{bmatrix} \boldsymbol{0}_{3\times12} & \boldsymbol{I}_3 \end{bmatrix}^{\mathrm{T}}, \tag{6}$$

as well as a matrix $\boldsymbol{G}$ coupling in noise components $\boldsymbol{w} \in \mathbb{R}^6$ proportional to angular acceleration

$$\boldsymbol{G} = \begin{bmatrix} \boldsymbol{I}_6 \cdot \frac{T_{\mathrm{s}}{}^2}{2} & \boldsymbol{I}_6 \cdot T_{\mathrm{s}} & \boldsymbol{0}_{6\times3} \end{bmatrix}^{\mathrm{T}} \tag{7}$$

where identity matrices and zero matrices with dimensions given in the subscript are denoted by $\boldsymbol{I}$ (always square) and $\boldsymbol{0}$ respectively. A timestep between samples (in the present configuration $1\,\mathrm{ms}$) is denoted by T_{s}. The resulting system equation is $\boldsymbol{x}(n+1) = \boldsymbol{A}\boldsymbol{x}(n) + \boldsymbol{B}\boldsymbol{p}_{\mathrm{b}}(n) + \boldsymbol{G}\boldsymbol{w}(n)$.

Incorporation of the kinematic chain happens in the output formulation. We define the output vector $\boldsymbol{z} \in \mathbb{R}^{15}$ as

$$\boldsymbol{z}(n) = \begin{bmatrix} \boldsymbol{\alpha}^{\mathrm{T}}(n) & \boldsymbol{p}_0^{\mathrm{T}}(n) & \boldsymbol{p}_1^{\mathrm{T}}(n) & \boldsymbol{p}_2^{\mathrm{T}}(n) \end{bmatrix}^{\mathrm{T}}, \tag{8}$$

leading to $\boldsymbol{z}(n) = \boldsymbol{h}(\boldsymbol{x}(n)) + \boldsymbol{v}(n)$, with a nonlinear output function $\boldsymbol{h}$ describing its connection with the system state and $\boldsymbol{v} \in \mathbb{R}^{15}$ modeling the measurement noise. Here, the angles are taken from the state and the positions are calculated according to the kinematic chain propagation explained above. As the conventional Kalman filter assumes fully linear systems, we employ the EKF approach through linearization of the output function $\boldsymbol{h}(\boldsymbol{x}(n))$ by computing its Jacobian matrix $\boldsymbol{H}(n) = \frac{\partial \boldsymbol{h}}{\partial \boldsymbol{x}}(n)$ where it is necessary for the Kalman update equations.

Using the introduced notions, we formulate the prediction step of our filter with the error covariance matrix $\boldsymbol{P}$ and the process noise covariance $\boldsymbol{Q} = \boldsymbol{G}\boldsymbol{G}^{\mathrm{T}}\sigma_\alpha^2$ as

$$\hat{\boldsymbol{x}}_{\mathrm{p}}(n+1) = \boldsymbol{A}\hat{\boldsymbol{x}}(n) + \boldsymbol{B}\boldsymbol{p}_{\mathrm{b}}(n), \tag{9a}$$

$$\boldsymbol{P}_{\mathrm{p}}(n+1) = \boldsymbol{A}\boldsymbol{P}(n)\boldsymbol{A}^{\mathrm{T}} + \boldsymbol{Q}, \tag{9b}$$

where the estimation is denoted by $\hat{(\cdot)}$ and a subscript p signifies the predictive variables. Taking the predicted state $\hat{\boldsymbol{x}}_{\mathrm{p}}$ we then nonlinearly calculate the estimated output $\hat{\boldsymbol{z}}$ that we are interested in. As a further inclusion of a priori knowledge, we limit the angles between the MC and PP as well as between the PP and MP by intervals around a typical physiological range of motion ($\theta_1 \in [-30°, 30°]$, $\psi_1 \in [-10°, 100°]$, $\psi_2 \in [0°, 110°]$). Hence we can guarantee a physically possible and consistent set of output poses once again mappable to an index finger.

Lastly, we use the preprocessed pose information $\boldsymbol{z}$ from the localization to correct our estimates by means of the Kalman gain matrix $\boldsymbol{K}$ which depends on the measurement covariance matrix $\boldsymbol{R}$ where the first three diagonal entries are $\sigma_{\mathrm{m},0}^2$, the fourth and fifth diagonal entry are $\sigma_{\mathrm{m},1}^2$, the sixth diagonal entry is $\sigma_{\mathrm{m},2}^2$ and the nine remaining diagonal values are $\sigma_{\mathrm{m},\boldsymbol{p}}^2$. The required equations are given by

$$\boldsymbol{K}(n) = \boldsymbol{P}_{\mathrm{p}}(n)\boldsymbol{H}^{\mathrm{T}}(n)\Big(\boldsymbol{H}(n)\boldsymbol{P}_{\mathrm{p}}(n)\boldsymbol{H}^{\mathrm{T}}(n) + \boldsymbol{R}\Big)^{-1}, \tag{10a}$$

$$\hat{\boldsymbol{x}}(n) = \hat{\boldsymbol{x}}_{\mathrm{p}}(n) + \boldsymbol{K}(n)\left(\boldsymbol{z}(n) - \hat{\boldsymbol{z}}(n)\right), \tag{10b}$$

$$\boldsymbol{M}(n) = \left(\boldsymbol{I}_{15} - \boldsymbol{K}(n)\boldsymbol{H}(n)\right), \tag{10c}$$

$$\boldsymbol{P}(n) = \boldsymbol{M}(n)\boldsymbol{P}_{\mathrm{p}}(n)\boldsymbol{M}^{\mathrm{T}}(n) + \boldsymbol{K}(n)\boldsymbol{R}\boldsymbol{K}^{\mathrm{T}}(n), \tag{10d}$$

which complete the description of the model-based filter.

3 Results

For this proof of concept work, the variance matrices were initialized with the examplary chosen, working values $\sigma_\alpha^2 = 60$, $\sigma_{\mathrm{m},0}^2 = 120$, $\sigma_{\mathrm{m},1}^2 = \sigma_{\mathrm{m},2}^2 = 400$ and $\sigma_{\mathrm{m},\boldsymbol{p}}^2 = 5$. The system is real-time capable with a small computational load of around 5% on a Ryzen 5 3600. In Figure 4, a full bending/unbending cycle taken from the resulting signals is shown for the examplary proximal sensor with the estimation results depicted in a darker color in relation to the respective reference. Instead of the first simulated cycle, during which a transient behaviour of the initial zero-state is present, an initially steady-state cycle is depicted. Figure 4A displays the pose estimations in relation to the simulated ground truth signals. The orientation is given in the local reference frame, which is why only the relevant pitch and yaw signals are plotted. The unwrapped global pose estimates are shown in reference to the stepped naive localization result (measurement for the EKF) in Figure 4B. Lastly, Figure 4C is an error plot of the x-position estimate

Tab. 1: Mean absolute errors of the shown cycle.

	MAE $[x\ y\ z]$ **(cm)**		**MAE** $[\varphi\ \theta\ \psi]$ **(°)**	
	EKF	**LP**	**EKF**	**LP**
MC	[0.1 0.1 0.3]	[1.3 1.2 1.2]	[6.4 3.5 6.6]	[12.3 6.0 10.2]
PP	[0.4 0.4 0.6]	[1.3 1.2 1.3]	[— 2.9 4.8]	[— 6.9 7.9]
MP	[0.7 0.8 0.7]	[1.0 1.3 1.4]	[— — 10.3]	[— — 8.6]

in relation to the ground truth. As an evaluation reference, the preprocessed signals were filtered with a simple lowpass filter (LP) using the scientific computing python library SciPy (Butterworth, 2nd order, 5 Hz). The resulting mean absolute error (MAE) for the estimated x-position is 0.6 cm compared to 1.3 cm for the naively filtered signal, which also exhibits more erratic behaviour. The other MAEs can be seen in Table 1.

4 Conclusions

In this paper, we introduced an approach of using an extended Kalman filter to include knowledge about the kinematic chain formed by a finger into a model-based magnetic tracking system. We simulated a hand performing a bending motion and considered resulting estimated pose signals as well as mean absolute error values. The system currently assumes a fixed working space for the localization, knowledge of the base position and three rotational degrees-of-freedom known by the first sensor, which makes at least a 2D sensor necessary at that point. A separate pose tracking of the base could enable the use of a 1D sensor at this point as well. While the local orientations of segments further along the chain suffer from potential error accumulation from the relative orientation computation during preprocessing, the results are promising overall. This motivates further research with several directions. One is the investigation of different simulated noise types and a comparison of the simulation with localization errors from future recordings. The usage of the filter for multiple fingers where the base position could be estimated from a combination of a higher number of sensors would be of high interest. We also assume further modeling of inter-finger relations and adaptation of the covariance matrices at runtime to be beneficial.

Author Statement

Research funding: This work was supported by the German Research Foundation (Deutsche Forschungsgemeinschaft, DFG) through the Collaborative Research Centre CRC 1261 “Magnetoelectric Sensors: From Composite Materials to Biomagnetic Diagnostics”. Conflict of interest: Authors state no conflict of interest. Informed consent: Informed consent has been obtained from all individuals included in this study. Ethical approval: The conducted research is not related to either human or animal use.

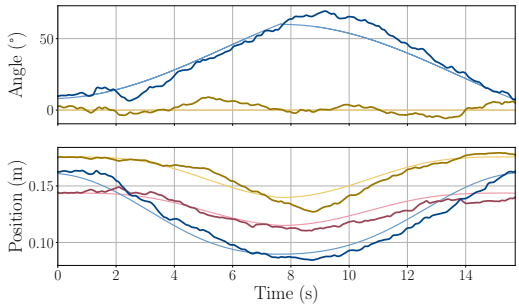

(A) Local pose estimate (dark) vs. ground truth (light).

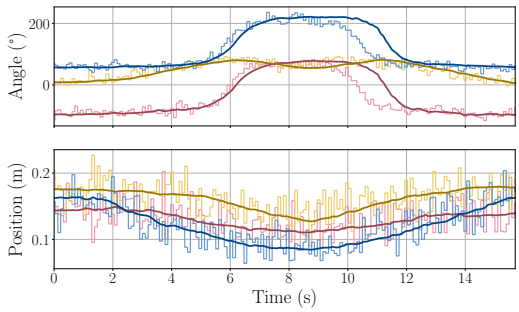

(B) Global pose estimate (dark) vs. unprocessed localization (light).

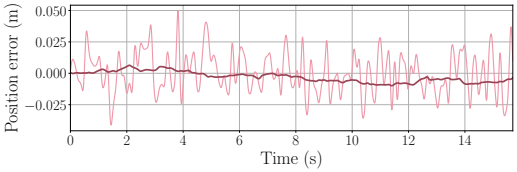

(C) Error to ground truth for model-based estimation (dark) vs. simple smoothing (light).

Figure 4: Results for the sensor at the PP with simulated bending and unbending of the index finger. Colors are red, yellow, and blue for x-/φ-, y-/θ-, and z-/ψ-signals, respectively.

References

[1] López-Casado C, Bauzano E, Rivas-Blanco I, Pérez-del-Pulgar CJ, Muñoz VF. A Gesture Recognition Algorithm for Hand-Assisted Laparoscopic Surgery. Sensors 2019;19(23):5182.

[2] Zhou T, Cabrera ME, Wachs J. Touchless Telerobotic Surgery — Is It Possible at All?. AAAI 2015;29(1).

[3] Bald C, Schmidt G. Processing Chain for Localization of Magnetoelectric Sensors in Real Time. Sensors 2021;21(16):5675.

[4] Bald C, Bergholz R, Schmidt G. Automatic Localization of an Ultrasound Probe with the Help of Magnetic Sensors. Curr Dir Biomed Eng 2022;8(2):317-320.

[5] Hoffmann J, Hansen C, Maetzler W, Schmidt G. A Concept for 6D Motion Sensing with Magnetoelectric Sensors. Curr Dir Biomed Eng 2022;8(2):451-454.

[6] Spetzler B, Bald C, Durdaut P, Reermann J, Kirchhof C, Teplyuk A, et. al. Exchange biased delta-E effect enables the detection of low frequency pT magnetic fields with simultaneous localization. Sci Rep 2021;11:5269.

[7] Buryanov A, Kotiuk V. Proportions of Hand Segments. Int J Morphol 2010;28(3):755-758.